

# Diagnosis of papillary thyroid carcinoma by $^1\text{H}$ NMR spectroscopy-based metabolomic analysis of whole blood

Tiantian Wang<sup>1,2,§</sup>, Zhigang Sun<sup>2,3,§</sup>, Yong Wang<sup>4</sup>, Feifei Li<sup>1</sup>, Xiaoming Zhou<sup>2</sup>, Xingsong Tian<sup>2</sup>, Shuqi Wang<sup>1,\*</sup>

<sup>1</sup>School of Pharmaceutical Sciences, Shandong University, Ji'nan, Shandong, China;

<sup>2</sup>Department of Thyroid and Breast Surgery, Shandong Provincial Hospital Affiliated to Shandong First Medical University, Ji'nan, Shandong, China;

<sup>3</sup>Department of Colorectal Surgery and State Key Lab of Molecular Oncology, Chinese Academy of Medical Sciences and Peking Union Medical College, Beijing, China;

<sup>4</sup>Department of Thyroid Surgery, The Second Affiliated Hospital of Zhejiang University College of Medicine, Hangzhou, Zhejiang, China.

**SUMMARY** The incidence rate of thyroid carcinoma, especially papillary thyroid carcinoma (PTC), has increased significantly over time. As a primary pathway for metastasis, the lymphatic system is an important prognostic factor for PTC patients. Although the metabolic changes in PTC patients have been investigated in extensive studies, few studies focused on the whole blood metabolic profiling of PTC patients. In this study, we investigated the  $^1\text{H}$  NMR-based metabolic profiles of whole blood samples that were obtained from healthy individuals and PTC patients, with or without lymph node metastasis. The estimation of the predictive potential of metabolites was evaluated using multivariate statistical analyses, which revealed that the whole blood carries information that is sufficient for distinguishing between PTC patients and healthy individuals. However, PTC patients were not well classified as positive or negative according to the lymph nodes. We did not find a metabolite that could discriminate the presence of lymph node metastasis. Further studies with larger sample sizes are needed to elucidate significant metabolites to indicate the presence of lymph node metastasis in patients with PTC.

**Keywords** Thyroid,  $^1\text{H}$  NMR spectroscopy, metabolomics, lymph node metastasis, papillary thyroid carcinoma

## 1. Introduction

Papillary thyroid carcinoma (PTC) is the most common type of thyroid cancer, representing 75-85% of all thyroid cancer cases (1). Surgery is the elective treatment for papillary thyroid carcinoma. Preoperative distinction between benign and malignant conditions is crucial to avoid overtreatment of patients and morbidity linked with an inappropriate surgery (2,3). Clinical research in thyroid pathology is focusing on the development of new diagnostic tools to improve the stratification of nodules that have biological, practical, and economic consequences on the management of patients. Ultrasound plays an increasingly important role in the diagnosis of the thyroid nodule, and the ultrasound-guided fine-needle aspiration biopsy (FNAB) has become the gold standard for preoperative judgment in thyroid carcinoma patients (4,5).

As an invasive diagnostic method, FNAB presents a certain risk of bleeding and a low possibility of needle tract metastasis. Patients receiving FNAB often require

surgery as soon as possible due to the risk of nodule enlargement or change in nodule nature. Therefore, the development of new diagnostic methods that could provide useful clinical information for the non-invasive diagnosis of the nature of thyroid nodules and lymph nodes is particularly important (6). We hope that this approach will decrease unnecessary repeated biopsies and surgical procedures.

Metabolomics is the systematic study of small molecular metabolites in cells, tissues, biofluids or cell culture medias, and provides tangible results regarding cellular processes or responses to environmental stresses (7). In general, cancer cells have an impaired energy metabolism, and metabolic intermediates typically accumulate in tumors (8). Metabolomics is now recognized as a powerful technique for identifying biomarkers and altering the metabolic pathways in cancer, including nucleotide synthesis, glycolysis, phospholipid and fatty acid metabolism, and amino acid metabolism (9,10). Metabolomics has been increasingly used to identify biomarkers for early diagnosis and

understanding the potential mechanisms of various cancers (11). In human studies, blood samples are used to capture a physiological average of the host's metabolic status and serum is routinely collected, which makes it a frequent and convenient sample for metabolomics studies.

However, the analysis of the serum metabolome does not consider the contribution of erythrocytes (12,13). Compelling evidence suggests a significant value of erythrocytes for metabolite profiling of whole blood in investigations of human health and diseases (13-16). The major advantage of whole blood analysis is that it provides access to both the plasma, serum, and red blood cell metabolome in one step and eliminates many of the pre-analytical processing problems with little additional effort compared to the traditionally used serum or plasma analysis (12,17). Thus, whole blood metabolomics offers an added opportunity to gain insights into additional metabolites and metabolic pathways.

In the present study, we investigated and compared the metabolomics characteristics of the whole blood from PTC patients and healthy controls using an untargeted metabolomics approach based on  $^1\text{H}$  NMR, coupled with multivariate statistical analyses. The metabolic differences according to the presence or absence of lymph node metastasis (LN) in patients with PTC were also investigated in our study, in the search for a potential novel prognostic biomarker.

## 2. Materials and Methods

### 2.1. Chemical Regents

Deuterium water ( $\text{D}_2\text{O}$ , 99.8%) was purchased from Tenglong Weibo Technology Co., Ltd. (Qingdao, China). High-performance liquid chromatography (HPLC) grade methanol, and 3-(trimethylsilyl)-1-propanesulfonic acid- $d_6$  sodium salt (DSS- $d_6$ ) was purchased from Sigma-Aldrich (St. Louis, MO, USA). All other chemical reagents were analytical grade.

### 2.2. Clinical samples and processing of whole blood

We collected whole blood samples from patients who underwent thyroid surgery ( $n = 80$ ) from the department of breast and thyroid surgery between January 2017 and October 2018, with prior ethical approval by the Institutional Ethics Committee, Shandong Provincial Hospital. The whole blood samples were collected from age matched healthy volunteers ( $n = 47$ ). All patients signed informed consent before participating in the study. The patients enrolled in this study did not receive any chemotherapy or radiation therapy before surgical treatment. The clinical details and pathological features of all study subjects are listed in Table 1. All samples were collected in EDTA-coated whole blood collection vials. Following collection, samples were

placed in an ice-water bath. 1 ml aliquots of blood were placed in cryogenic tubes and immediately flash frozen in liquid nitrogen before being stored at  $80^\circ\text{C}$ . Whole blood samples were stored at  $80^\circ\text{C}$  until further experimentation.

### 2.3. Sample processing for NMR spectroscopy

The reagents were kept ice-cold before use. To extract the metabolites, 400  $\mu\text{L}$  of whole blood was mixed with cold methanol in a 1:2 sample/methanol (v/v) ratio. All sample solutions were then vortexed for 30 s, and sonicated for 2 min at  $4^\circ\text{C}$ . The mixtures were centrifuged at 14,600 rpm for 20 min to pellet the proteins and cell debris (12). The clear aqueous solutions were transferred to fresh vials and evaporated to dryness at  $45^\circ\text{C}$  in a speedvac concentrator (SPD2010 Integrated SpeedVac, ThermoFisher Scientific, USA). The dried samples were mixed with 600  $\mu\text{L}$  phosphate buffer containing 0.5 mM DSS- $d_6$ , and the pH was adjusted to 7.0 with NaOH and/or HCl. Then, we spun the samples to sediment any residue, and the supernatants were transferred to 5 mm NMR tubes for analysis.

### 2.4. NMR experiments

All one-dimensional  $^1\text{H}$  NMR spectra were acquired using a Bruker Avance III 600 MHz NMR spectrometer (Bruker GmbH, Rheinstetten, Germany) operating at

**Table 1. The clinical information and pathological features of all patients**

	All Patients	LN metastasis	No LN metastasis
Age (years, range)			
$\geq 45$	41	19	22
$< 45$	39	25	14
Sex			
Male	27	24	3
Female	53	20	33
TNM stage			
I	27	0	27
II	9	0	9
III	25	25	0
IV	19	19	0
Primary tumor numbers			
1	61	30	31
$> 1$	19	14	5
Primary tumor numbers (tumor size $\leq 10\text{mm}$ )			
1	35	13	22
$\geq 1$	13	8	5
Primary tumor size (mm)			
$\leq 10$	32	20	12
$> 10$	48	24	24
Primary tumor localization			
One side	69	35	34
Both side	11	9	2

a proton frequency of 600.1 MHz, equipped with a cryoprobe at 298 K. The  $^1\text{H}$  NMR experiments were performed using the Carr-Purcell-Meiboom-Gill (CPMG) pulse sequence with water pre-saturation to remove broad signals of molecules. The CPMG spectra were recorded with 64,000 time domain data points, a 20.0 ppm spectral width, 32 scans, and a relaxation delay of 5 s. All data were manually phased, and baseline corrected. All resonances of the metabolites present in  $^1\text{H}$  NMR were confirmed by referring to the Biological Magnetic Resonance Bank (BMRB), Human Metabolome Database (HMDB), published research articles, and by comparing with standard data.

### 2.5. Data processing and analysis

The data were preprocessed with MestReNova 12.0 (Mestrelab Research SL, Santiago de Compostela, Spain), and manual phasing adjustment of the raw NMR data (FID), and the post-processing consisted of Fourier transformation, phasing and baseline correction, cutting off the solvent peak (water peak, 4.75-4.91 ppm), and normalization. We then performed the piecewise binning; the spectral region from 1.1 to 9.00 ppm was segmented into 148 intervals with an equal width of 0.05 ppm. The data were exported, converted to Excel format, examined, and removed from the solvent peak section.

The normalized NMR data in Excel format were imported into statistical software SIMCA-P (Version 14.0; Umetrics AB, Umea, Sweden) for multivariate statistical analysis, including principal component analysis (PCA), partial least squares discriminant analysis (PLS-DA), and orthogonal projection to latent structure (OPLS) analysis. PCA was first performed to determine possible outliers. The model type selected was PCA-X. We used the scale selected Par data processing mode, completed automatic fitting, and examined the abnormal points. Generally, two times the red line value was used as the abnormal point standard. If there were abnormal points, we deleted the corresponding data in the comprehensive analysis and checked the fit again. After no outlier points remained, the model type selected PLS-DA to build the PLS-DA model, and the order of the samples in the dataset was randomized. The discriminant version of the partial least squares regression (PLS-DA) with a default k-fold cross validation procedure was used to determine the differences between the groups.

**Perturbation testing of the model:** The PLS-DA was cross-validated by a permutation analysis (200 times). All points should be at the right of the highest point, with the data separated between groups and clustered within groups. We calculated the  $R^2$  and  $Q^2$  values.

The OPLS model was built following the same procedure to obtain good separation between different groups. The  $R^2$  and  $Q^2$  obtained after fitting indicated

the parameters of interpretability and the predictability of the model, respectively, which were used to evaluate the quality of the model. To identify the significant spectral peaks, variable importance in the projection (VIP) of  $> 1$  was considered as a criterion for differences between different groupings, which was analyzed and taken as a coefficient from the OPLS model. The identified metabolites were chosen as discriminating ones, which met the conditions of  $\text{VIP} > 1$ . We generated an S-plots graph, and the variables of the two diagonals of the S-shape were considered as differential metabolites. According to the histogram of the VIP values and S-plots graph to preliminary screen differential metabolites, we used the MetaboAnalyst database to judge the types of metabolites and predict the metabolic pathways and intermediate metabolites in the metabolic pathways (18-20).

## 3. Results

### 3.1. $^1\text{H}$ NMR metabolic profiles of whole blood samples

For the  $^1\text{H}$  NMR spectra of whole blood, the CPMG pulse sequence was used to suppress the resonances from macromolecules, such as proteins and lipoproteins. Typical  $^1\text{H}$  NMR spectra of whole blood samples are shown in Figure 1. The ppm scale was expanded to focus on the range of 0.8-9.0 ppm. The resonances attributed to a series of endogenous compounds were identified according to the literature and some public databases (HMDB and BMRB). These peaks were further assigned as lactate, lysine, acetic acid, arginine, glutamic acid, methionine, proline, 3-hydroxybutyric acid, aspartate, tyrosine, 1-methylhistidine, creatine, D-glucose, acetoacetate, L-threonine, L-ornithine, isopropyl alcohol, L-histidine, L-phenylalanine, hypoxanthine, and formate.

### 3.2. Multivariate statistical analysis

To perform a comprehensive comparison of the metabolic profiles among the groups, we employed PCA and O2PLS-DA with the first two principal components (Figure 2). The PCA scores plot showed that the PTC groups (LN-negative and LN-positive) and the normal group samples were scattered into different regions, whereas overlaps between the LN-negative and LN-positive subjects were also observed in the PCA score plots. The majority of the samples were in the 95% confidence interval. Therefore, all the samples were used in the following analysis to ensure the maximum information.

To further identify the metabolic characteristics of the patients, pairwise OPLS-DA was performed. Obvious separations between the normal group and PTC group, the normal group and LN-negative group, the normal group and LN-positive group, and the

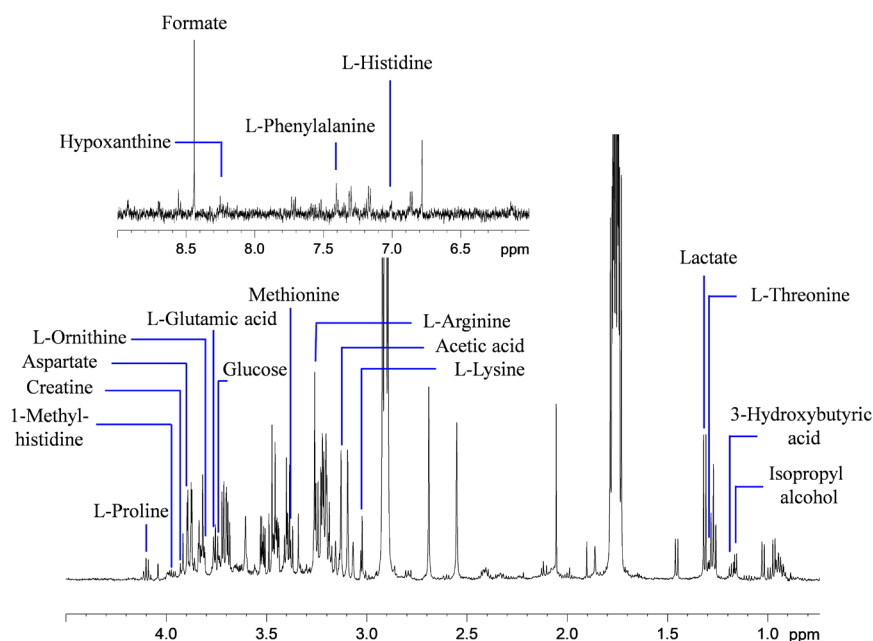


Figure 1. Representative whole blood 600 MHz  $^1\text{H}$  NMR spectra.

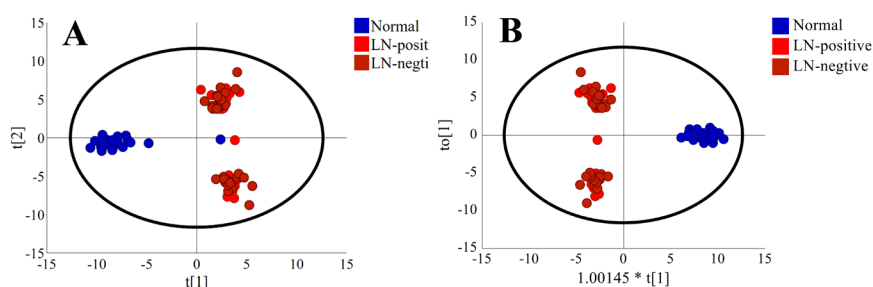


Figure 2. Metabolic profiling between the LN-negative PTC group, LN-positive PTC group and normal controls. A, principal component analysis (PCA) scores plot and B, O2PLS-DA scores plot.

LN-negative group and LN-positive (Figure 3) group were observed. A separation between the normal group and the PTC was shown in Figure 3A. The model parameters ( $R^2 = 0.954$ ,  $Q^2 = 0.914$ ) demonstrated a good quality of the obtained OPLS model. In the S-plot (Figure 3E), the variables far away from the center of the plot were assumed to have a greater contribution to the model separation. Whole blood metabolite expression patterns were observed in PTC patients and healthy controls, respectively. The pairwise PLS-DA between PTC patients and healthy controls revealed a clear separation with  $R^2Y$  (cum) = 0.77,  $Q^2$  (cum) = 0.61 and  $R^2Y$  (cum) = 0.75,  $Q^2$  (cum) = 0.61, respectively (Figure 3).

To identify the significantly distinguishing metabolites in discriminating between LN-negative and LN-positive PTC patients, further multivariate statistical analysis was performed. OPLS-DA was

performed to separate the patients into two groups for each comparison. To the best of our knowledge, this is the first study to characterize the whole blood metabolic profile of PTC with or without LN, which is useful for identifying potential biomarkers and understanding the underlying molecular mechanism. However, the OPLS-DA score plots did not separate the two groups clearly for all three comparisons. When the patients were classified into LN-negative and LN-positive, the OPLS-DA score plot exhibited nonseparation between the two groups (Figure 3D).

We first identified 48 metabolites according to their corresponding chemical shift and multiplicity. The altered metabolite level in the whole blood of PTC patients and healthy controls was characterized. Based on the statistical analysis of the results ( $p < 0.05$  and  $\text{VIP} > 1$ ), 20 metabolites were identified as potential biomarkers for PTC and the color change for

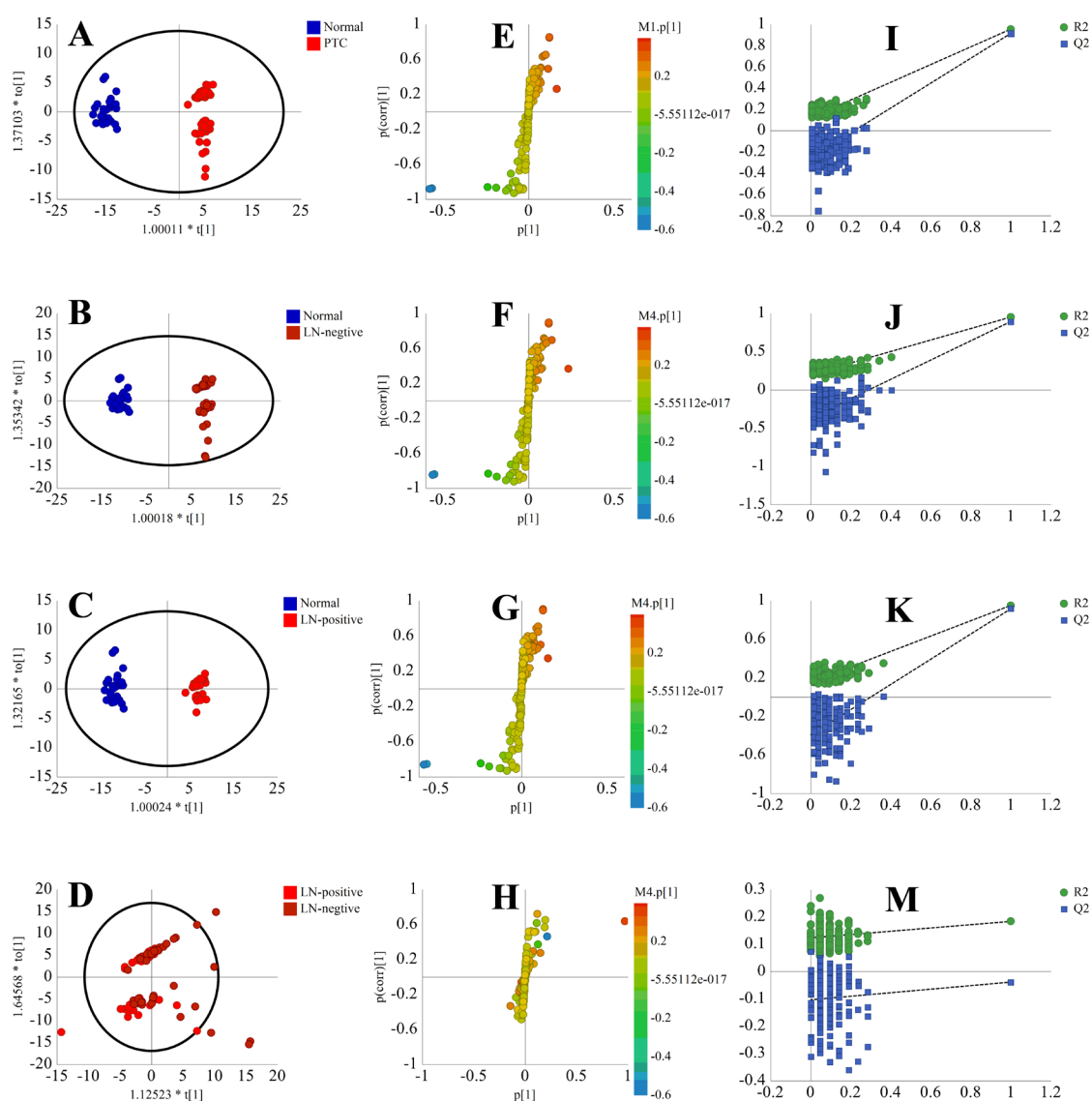


**Figure 3. Metabolic profiling between the PTC and normal controls.** A, B, C, and D are the orthogonal projection to latent structure discriminant analysis (OPLS-DA) scores plots between the PTC and normal controls, LN-negative and normal controls, LN-positive and normal controls, and LN-negative and LN-positive. E, F, G, and H are S-plots of the OPLS-DA model of the PTC and normal controls, LN-negative and normal controls, LN-positive and normal controls, and LN-negative and LN-positive, the variables that lie far away from the center of the plot were assumed to have a greater contribution to the model classification. I, J, K, and M are validation plots of the OPLS-DA model of the PTC and normal controls, LN-negative and normal controls, LN-positive and normal controls, and LN-negative and LN-positive using a permutation test that was randomly permuted 200 times. The explained variance (R2X) and predictivity (Q2Y) of the constructed model are indicated on the far right and remain higher than those of the 200 permuted models to the left.

the key metabolites according to the VIP-parameter is shown in Figure 3E and Table 2. We also evaluated the significance of the altered metabolites level in the LN-negative and LN-positive groups as compared to healthy subjects (Table 2). Compared to the normal controls, the concentrations of tyrosine, lactate, lysine, acetic acid, arginine, glutamic acid, methionine, hydroxybutyric acid, aspartate, tyrosine, acetoacetate, threonine, histidine, hypoxanthine, and formate decreased in PTC patients, whereas the concentrations of isobutyric acid, proline, 1-methylhistidine, creatine, glucose, ornithine, and isopropyl alcohol increased.

To evaluate the performance of each altered

metabolite in distinguishing PTC from healthy subjects; we analyzed the diagnostic accuracy through receiver operating characteristic (ROC) curves analysis. The diagnostic accuracy in the form of the area under the ROC curve (AUC) was evaluated in the datasets of healthy vs. PTC, healthy vs. LN-negative, and healthy vs. LN-positive patients (Table 3). The metabolites were also used to construct an independent model, and we found that isobutyric acid, lactate, lysine, arginine, glutamic acid, methionine, proline, aspartate, tyrosine, creatine, glucose, threonine, ornithine, isopropyl alcohol, and formate performed with good diagnostic potential with AUC scores of more than 0.9 in all

**Table 2. The differential metabolites among all papillary thyroid carcinoma (PTC) patients, LN-positive PTC patients, LN-negative PTC patients, and normal controls**

Metabolites	Chemical shift <sup>a</sup> (ppm, multiplicity)	PTC vs. Normal			LN-positive vs. Normal			LN-negative vs. Normal		
		VIP <sup>b</sup>	P <sup>c</sup>	FC <sup>d</sup>	VIP <sup>b</sup>	P <sup>c</sup>	FC <sup>d</sup>	VIP <sup>b</sup>	P <sup>c</sup>	FC <sup>d</sup>
Lactate	1.32 ( <i>d</i> )	1.141	9.45E-08	27.187	1.0958	6.54E-06	26.416	1.4698	6.48E-10	28.14
L-Lysine	3.03 ( <i>t</i> )	2.0087	9.50E-04	0.011598	1.8146	5.45E-19	0.014733	1.7784	1.52E-16	0.0077247
Acetic acid	3.11 ( <i>d</i> )	1.3528	3.29E-03	0.40239	1.1992	5.46E-07	0.43641	1.3331	5.40E-08	0.36032
L-Arginine	3.25 ( <i>t</i> )	1.602	1.12E-02	0.25497	1.5119	1.81E-11	0.23638	1.4474	1.43E-09	0.27797
L-Glutamic acid	3.76 ( <i>q</i> )	1.8954	2.62E-25	0.19049	1.7676	1.79E-17	0.2036	1.7881	7.82E-17	0.17427
Methionine	3.38 ( <i>s</i> )	2.0955	3.07E-36	0.051506	1.9201	3.33E-23	0.061593	1.9079	3.37E-21	0.039035
L-Proline	4.10 ( <i>m</i> )	1.0941	3.59E-07	9.7312	1.1348	2.67E-06	10.215	1.2316	8.19E-07	9.1315
3-Hydroxybutyric acid	1.22 ( <i>d</i> )	1.2645	1.84E-09	0.2245	1.154	1.69E-06	0.22264	1.1268	9.15E-06	0.2268
Aspartate	3.90 ( <i>q</i> )	2.0767	6.34E-35	0.091451	1.9829	1.67E-26	0.05952	1.8387	1.74E-18	0.13094
Tyrosine	4.42 ( <i>m</i> )	2.0821	2.70E-35	0.0077964	1.8898	7.46E-22	0.0063454	1.837	1.99E-18	0.0095911
1-Methylhistidine	3.98 ( <i>m</i> )	1.1721	3.72E-08	3.7893	1.1772	9.55E-07	3.5902	1.3416	4.21E-08	4.0355
Creatine	3.93 ( <i>s</i> )	1.4811	2.98E-13	2.5773	1.5453	4.28E-12	2.5713	1.5156	1.16E-10	2.5848
D-Glucose	3.72 ( <i>m</i> )	2.0161	3.56E-31	3.6886	1.9788	2.92E-26	3.8243	1.9263	4.92E-22	3.5207
L-Threonine	1.30 ( <i>d</i> )	1.6894	3.08E-18	0.38636	1.7044	1.11E-15	0.38161	1.5688	1.30E-11	0.39223
L-Ornithine	3.81 ( <i>t</i> )	1.5034	1.04E-13	2.8769	1.3843	2.25E-09	2.7964	1.3898	9.70E-09	2.9764
Isopropyl alcohol	1.17 ( <i>d</i> )	1.1943	1.87E-08	3.2248	1.308	2.60E-08	2.5971	1.3666	1.99E-08	4.0013
L-Histidine	7.09 ( <i>d</i> )	1.5729	2.99E-15	0.22942	1.5081	2.12E-11	0.2296	1.5272	7.33E-11	0.2292
L-Phenylalanine	7.44 ( <i>d</i> )	1.1865	2.39E-08	0.30858	1.0246	2.96E-05	0.38102	1.5358	5.17E-11	0.219
Hypoxanthine	8.23 ( <i>s</i> )	0.94239	1.59E-05	164.71	1.0839	8.51E-06	163.11	1.0141	8.43E-05	166.52
Formate	8.45 ( <i>s</i> )	2.0866	1.32E-35	0.043805	1.9294	1.21E-23	0.032461	1.8646	1.96E-19	0.057839

<sup>a</sup>Multiplicity: *s* singlet, *d* doublet, *t* triplet, *q* quartet, *m* multiplet. <sup>b</sup>Variable importance in the projection was obtained from OPLS model. <sup>c</sup>*p*-value obtained from Student's *t*-test. <sup>d</sup>Fold change (FC) was calculated as a binary logarithm of the average mass response (normalized peak area) ratio between PTC versus normal controls, LN-positive versus normal controls or between LN-negative versus normal controls.

**Table 3. The details of the ROC curves of all significantly altered metabolites in different groups**

Metabolites	PTC vs. Normal		LN-negative vs. Normal		LN-positive vs. Normal	
	AUC	95% CI	AUC	95% CI	AUC	95% CI
Lactate	0.980	0.937-1.0	0.983	0.939-1.0	0.978	0.929-1.0
L-Lysine	0.982	0.953-0.999	0.985	0.958-1.0	0.979	0.945-0.999
Acetic acid	0.844	0.823-0.941	0.867	0.761-0.948	0.826	0.711-0.917
L-Arginine	0.954	0.893-0.991	0.951	0.887-0.99	0.957	0.901-0.995
L-Glutamic acid	0.964	0.919-0.996	0.969	0.923-1.0	0.960	0.908-1.0
Methionine	0.974	0.918-1.0	0.976	0.925-1.0	0.972	0.913-1.0
L-Proline	0.921	0.841-0.978	0.922	0.846-0.988	0.921	0.843-0.985
3-Hydroxybutyric acid	0.869	0.787-0.924	0.876	0.795-0.95	0.862	0.784-0.94
Aspartate	0.961	0.913-0.996	0.949	0.844-0.993	0.970	0.921-1.0
Tyrosine	0.973	0.93-1.0	0.970	0.923-1.0	0.975	0.937-1.0
1-Methylhistidine	0.875	0.798-0.942	0.890	0.794-0.959	0.862	0.772-0.944
Creatine	0.904	0.839-0.958	0.911	0.829-0.978	0.899	0.813-0.979
D-Glucose	0.986	0.966-1.0	0.989	0.958-1.0	0.984	0.955-1.0
L-Threonine	0.938	0.868-0.988	0.925	0.83-0.988	0.949	0.88-0.996
L-Ornithine	0.940	0.857-0.993	0.943	0.871-0.955	0.938	0.85-0.996
Isopropyl alcohol	0.935	0.853-0.984	0.945	0.872-0.997	0.926	0.838-0.989
L-Histidine	0.895	0.809-0.952	0.898	0.815-0.964	0.891	0.806-0.954
L-Phenylalanine	0.889	0.823-0.941	0.926	0.864-0.987	0.858	0.766-0.932
Hypoxanthine	0.680	0.581-0.78	0.767	0.649-0.871	0.609	0.488-0.733
Formate	0.980	0.942-1.0	0.975	0.926-1.0	0.984	0.956-1.0

PTC patients compared with the healthy subjects. To clearly demonstrate these differences, scatter plots were constructed to illustrate the relative concentration (Figure 4). In the LN-negative and LN-positive subjects, the significance of all these metabolites were similarly found in PTC patients.

### 3.3. Metabolic pathway analysis

A pathway analysis provides useful information about the biological roles of metabolites, which can further provide insights into the pathogenesis and mechanisms of a specific disease. To further explore the metabolic

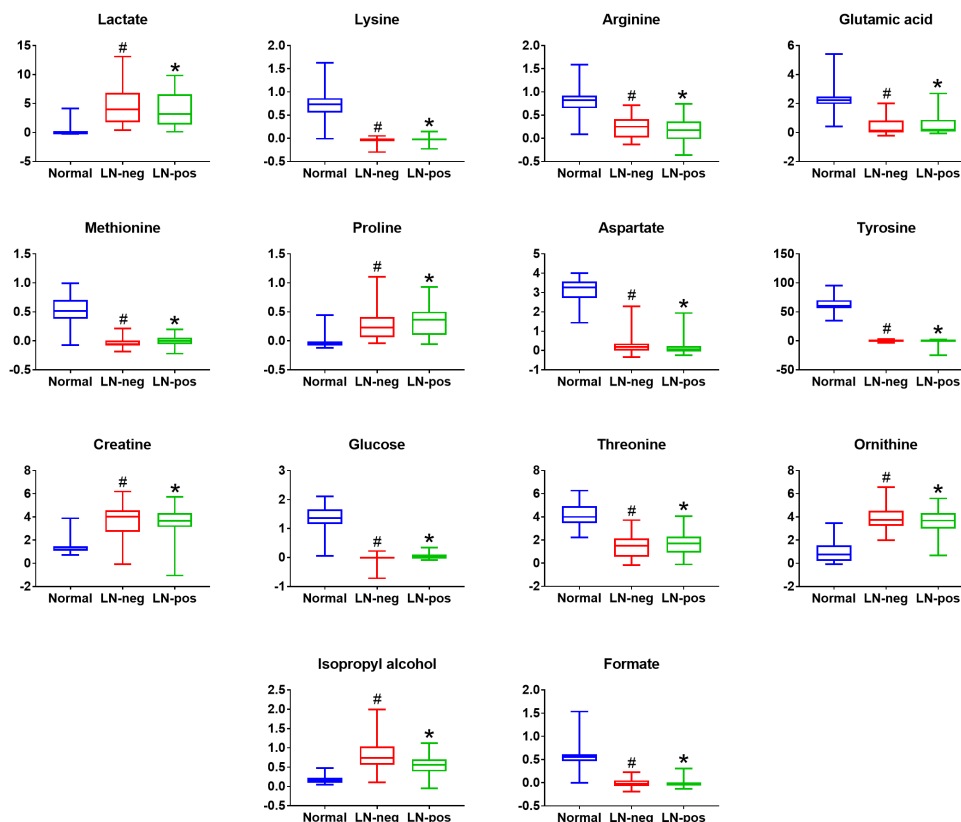


**Figure 4.** Scatter plots illustrating discrimination among normal controls, LN-negative and LN-positive PTC patients. The Y axis represents the relative abundance of NMR signals (normalized to the total peaks). \* $p < 0.01$  from the LN-positive PTC versus normal controls; # $p < 0.01$  from the LN-negative PTC versus normal controls.

**Table 4.** The results from pathway analysis using the software package KEGG graph

Pathway Name	Hits	$P$	$-\log(p)$	Holm $p$	FDR	Impact
Histidine metabolism	4	3.3309E-5	10.31	0.0027313	9.3265E-4	0.22131
Arginine biosynthesis	4	1.8628E-5	10.891	0.0015461	7.8236E-4	0.2538
Phenylalanine, tyrosine and tryptophan biosynthesis	2	9.3496E-4	6.975	0.074797	0.015707	1.0
Arginine and proline metabolism	5	8.0243E-5	9.4304	0.0064997	0.0016851	0.34441
Phenylalanine metabolism	2	0.006693	5.0067	0.52875	0.086182	0.35714
Pyruvate metabolism	2	0.031315	3.4637	1.0	0.23913	0.14463
Alanine, aspartate and glutamate metabolism	2	0.048932	3.0173	1.0	0.31618	0.42068

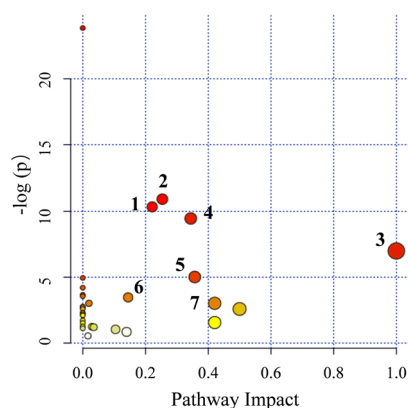


**Figure 5.** The impact of metabolic pathways in PTC. 1, Histidine metabolism; 2, Arginine biosynthesis; 3, Phenylalanine, tyrosine and tryptophan biosynthesis; 4, Arginine and proline metabolism; 5, Phenylalanine metabolism; 6, Pyruvate metabolism; 7, Alanine, aspartate and glutamate metabolism. The size and color of each circle is based on the pathway impact value and the  $p$ -value, respectively.

pathways that are involved in the regulation of PTC formation, the detected differential metabolites and their potential metabolic pathways were analyzed using KEGG graph software and the KEGG database. To explore metabolic pathway influences between the normal group and PTC group, pathway analysis performed by MetaboAnalyst 4.0, which combined results from powerful pathway enrichment analysis with the topology analysis.

Metabolic pathway analysis revealed that over 31 pathways were influenced (Table 4 and Figure 5). An impact value  $> 0.1$  and a hit value  $> 2$  were used as the threshold to identify the significantly altered metabolic pathways (21). Accordingly, seven potential target pathways were identified in whole blood samples, including arginine biosynthesis; histidine metabolism; arginine and proline metabolism; butanoate metabolism;

phenylalanine, tyrosine and tryptophan biosynthesis; the synthesis and degradation of ketone bodies, phenylalanine metabolism; alanine, aspartate and glutamate metabolism; and tyrosine metabolism. The pathways details are displayed in Table 4.

#### 4. Discussion

Currently, fine-needle aspiration (FNA) cytology has been used on a growing number of patients to determine the benign or malignant nature of their thyroid nodules and enlarged lymph nodes before surgery. The natures of some nodules and lymph nodes are indeterminate with FNAB alone. Once nodules and lymph nodes are identified as uncertain in nature, this will affect the most appropriate management strategy (22-24). After surgery, only approximately 80% of these thyroid nodules are malignant, which indicates that about 20% of patients with benign nodules were undergoing unnecessary thyroidectomy (25). The prediction of PTC, including the risk prediction of lymph node metastasis, is not only significant for guiding the indication of surgery to improve prognosis but also more significant for avoiding overtreatment and improving the quality of life.

In the present study, we investigated and identified the metabolic characteristics of the whole blood samples from PTC patients and healthy controls using <sup>1</sup>H NMR-based metabolomics and multivariate pattern recognition analytical techniques for the first time. Our results revealed that the metabolic phenotype of PTC patients' blood was significantly different from that of healthy controls' blood. In detail, 20 metabolites were significantly altered in PTC patients compared with those in the healthy controls. The presence of LN in patients with PTC was also distinguished for the first time, where no clear associations was observed. Compared with the published reports of the metabolic profiling of PTC (26-29), we focused on the metabolite profiling of whole blood in investigations of human health and PTC patients. The identified metabolites may be the potential factors for the diagnosis and prognosis of PTC patients. They also were valuable in understanding the molecular mechanisms in the process of PTC.

The identification of specific metabolites displaying altered levels of their associative metabolic pathways can improve the understanding of the biological and pathological aspects involved in the process from normal to an eventually cancerous state. Altered pathways include changes in arginine biosynthesis; histidine metabolism; arginine and proline metabolism; butanoate metabolism; phenylalanine, tyrosine and tryptophan biosynthesis; synthesis and degradation of ketone bodies, phenylalanine metabolism; alanine, aspartate and glutamate metabolism; and tyrosine metabolism.

Growth of cancer cells is rapid and divided into short cycles, requiring a higher energy supply to complete more biosynthesis, which requires reprogramming of

biochemical pathways to alter the metabolism of the cells. These alterations include increased glucose and glutamine uptake, lactate production, and abnormal biosynthesis of nucleic acids, proteins, and lipids (30). Deja *et al.* found that metabolic differences not only between thyroid cancer and normal tissues but also between different types of thyroid lesions, reflected the sensitivity of the metabolomic fluctuations. They concluded that the metabolic changes in thyroid carcinoma are mainly related to osmotic regulators, citrate, and amino acids that provide produce the TCA cycle (31).

In the present study, a decreased glucose level and increased lactate level in the LN-negative and LN-positive PTC groups compared to those in the healthy control group indicated that the energy supply pattern shifted from aerobic to anaerobic metabolism (Figure 4) (26,29). Creatine, phosphocreatine, and creatinine, through the creatine kinase reaction, played important roles in maintaining a constant ATP level (32). During arginine and proline metabolism, phosphocreatine and creatinine are the breakdown products of creatine, which reacts with ATP under the catalysis of creatine kinase (33).

In our results, the increased level of creatine in the PTC group suggested a disruption of their conversion to ATP, which may then cause an ATP depletion, and consequently may block the supply of energy in PTC patients. Aspartate, asparagine, glutamine, and glutamate are all involved in the alanine, aspartate, and glutamate metabolism. The decreased levels of glutamate and aspartate in PTC patients suggested that the generation from glutamine to glutamate was obstructed. The decrease in glutamate led to the distribution of the TCA cycle and the formation of glutathione.

The results of metabolomic studies are more contrasting regarding amino acids (34). Among the biomarkers identified, amino acids, such as glutamine, lysine, valine, and arginine were inversely associated with hepatocellular and prostate cancer risk in some prospective metabolomic studies (35-38). Li *et al.* analyzed normal thyroid and matched tumor tissues obtained from 16 patients and concluded that the metabolic components of PTC are characterized by increased glycolysis and inhibition of the tricarboxylic acid cycle, and an abnormal metabolism of carcinogenic amino acids, choline, and lipids (39).

In a similar study, Miccoli *et al.* studied 72 patients who underwent total thyroidectomy. They found that the thyroid tumor sample spectra had higher levels of lactate and acetylcholine, and lower levels of lipids and alanine than the normal sample (40). Our study showed that amino acid differences were mainly reflected in tyrosine, lysine, arginine, glutamic acid, methionine, aspartate, tyrosine, threonine, ornithine, and histidine. Future studies should focus on amino acid metabolisms, and on elucidating the mechanisms underlying the process of

LN of PTC before the clinical application of the FNA.

The prediction of PTC is not only significant for guiding the indication of surgery to improve prognosis but also for avoiding overtreatment and improving the quality of life. Metabolomics has the potential to change our existing understanding of the molecules involved in thyroid carcinoma, thus becoming a new diagnostic approach, providing metabolomic support for the preoperative evaluation of the nature of thyroid nodules, such as FNAB. Metabolomics can also improve our understanding of the process of cancer development and novel biomarkers. In the future, we hope to have more samples and more accurate metabolomic studies for the lymph node metastasis of papillary thyroid carcinoma, to realize the auxiliary judgment for the presence or absence of lymph node metastasis through the quantification of metabolites and metabolic pathways.

In conclusion, we were able to distinguish PTC patients from healthy controls with a high level of accuracy based on principal component analysis and linear discriminant analysis of the <sup>1</sup>H NMR metabolomic data obtained from whole blood samples. We first investigated the metabolic profiles between the LN-negative and LN-positive cancer subjects. No metabolite was found that could discriminate the presence of LN metastasis. The metabolic information obtained by <sup>1</sup>H NMR might play a significant role in screening biomarkers and in the early diagnosis of PTC cancer. Further studies with larger sample sizes are needed to elucidate significant metabolites to indicate the presence of LN metastasis in patients with PTC.

### Acknowledgements

This work was supported by the Key Research, Development Program of Shandong Province (2017GSF218049) and Young Scholars Program of Shandong University (2018WLJH93), and Shandong medical and health science and technology development program (2017WS098).

### References

- Chen M, Shen M, Li Y, Liu C, Zhou K, Hu W, Xu B, Xia Y, Tang W. GC-MS-based metabolomic analysis of human papillary thyroid carcinoma tissue. *Int J Mol Med*. 2015; 36:1607-1614.
- Haugen BR. 2015 American Thyroid Association Management Guidelines for Adult Patients with Thyroid Nodules and Differentiated Thyroid Cancer: What is new and what has changed? *Cancer*. 2017; 123:372-381.
- Chan DS, Gong K, Roskies M, Forest V, Hier MP, Payne RJ. Re-visiting the ATA 2015 sonographic guidelines - who are we missing? A retrospective review. *J Otolaryngol Neck Surg*. 2018; 47:1-6.
- Pagni F, Limperio V, Bono F, Garancini M, Roversi G, De Sio G, Galli M, Smith AJ, Chinello C, Magni F. Proteome analysis in thyroid pathology. *Expert Rev Proteomics*. 2015 12:375-390.
- Cooper DS, Doherty GM, Haugen BR, Kloos RT, Lee SL, Mandel SJ, Mazzaferri EL, Mciver B, Pacini F, Schlumberger M. Revised American Thyroid Association Management Guidelines for Patients with Thyroid Nodules and Differentiated Thyroid Cancer. *Thyroid*. 2009; 19:1167-1214.
- Wojtowicz W, Zabek A, Deja S, Dawiskiba T, Pawelka D, Glod M, Balcerzak W, Mlynarz P. Serum and urine <sup>1</sup>H NMR-based metabolomics in the diagnosis of selected thyroid diseases. *Sci Rep*. 2017; 7:9108.
- German JB, Hammock BD and Watkins SM. Metabolomics: building on a century of biochemistry to guide human health. *Metabolomics*. 2005; 1:3-9.
- Strand E, Tangen IL, Fasmer KE, Jacob H, Halle MK, Hoivik EA, Delvoux B, Trovik J, Haldorsen IS, Romano A. Blood Metabolites Associate with Prognosis in Endometrial Cancer. *Metabolites*. 2019; 9:302.
- Bitencourt AGV, Goldberg J, Pinker K, Thakur SB. Clinical applications of breast cancer metabolomics using high-resolution magic angle spinning proton magnetic resonance spectroscopy (HRMAS <sup>1</sup>H MRS): systematic scoping review. *Metabolomics*. 2019; 15:148.
- Beger RD. A review of applications of metabolomics in cancer. *Metabolites*. 2013; 3:552-574.
- Wang H, Wang L, Zhang H, Deng P, Chen J, Zhou B, Hu J, Zou J, Lu W, Xiang P, Wu T, Shao X, Li Y, Zhou Z, Zhao YL. <sup>1</sup>H NMR-based metabolic profiling of human rectal cancer tissue. *Mol Cancer*. 2013; 12:121.
- Nagana Gowda GA, Raftery D. Whole blood metabolomics by <sup>1</sup>H NMR spectroscopy provides a new opportunity to evaluate coenzymes and antioxidants. *Anal Chem*. 2017; 89:4620-4627.
- Stringer KA, Younger JG, McHugh C, Yeomans L, Finkel MA, Puskarich MA, Jones AE, Trexel J, Karnovsky A. Whole blood reveals more metabolic detail of the human metabolome than serum as measured by <sup>1</sup>H-NMR spectroscopy: Implications for sepsis metabolomics. *Shock*. 2015; 44:200-208.
- Catalan U, Rodriguez M, Ras M, Macia A, Mallol R, Vinaixa M, Fernandezcastillejo S, Valls R, Pedret A, Griffin JL. Biomarkers of food intake and metabolite differences between plasma and red blood cell matrices: a human metabolomic profile approach. *Mol Biosyst*. 2013; 9:1411-1422.
- Chaleckis R, Ebe M, Pluskal T, Murakami I, Kondoh H, Yanagida M. Unexpected similarities between the *Schizosaccharomyces* and human blood metabolomes, and novel human metabolites. *Mol Biosyst*. 2014; 10:2538-2551.
- Chaleckis R, Murakami I, Takada J, Kondoh H, Yanagida M. Individual variability in human blood metabolites identifies age-related differences. *Proc Natl Acad Sci*. 2016; 113:4252-4259.
- McHugh CE, Flott TL, Schooff CR, Smiley Z, Puskarich MA, Myers DD, Younger JG, Jones AE, Stringer KA. Rapid, reproducible, quantifiable NMR metabolomics: Methanol and methanol: Chloroform precipitation for removal of macromolecules in serum and whole blood. *Metabolites*. 2018; 8:93.
- Chong J, Wishart DS, Xia J. Using MetaboAnalyst 4.0 for comprehensive and integrative metabolomics data analysis. *Curr Protoc Bioinforma*. 2019; 68:e86.
- Chong J, Yamamoto M, Xia J. MetaboAnalystR 2.0: From raw spectra to biological insights. *Metabolites*. 2019; 9:57.
- Chong J, Xia J. MetaboAnalystR: an R package for

- flexible and reproducible analysis of metabolomics data. *Bioinformatic*. 2018; 34:4313-4314.
21. Jin H, Zhu B, Liu X, Jin J, Zou H. Metabolic characterization of diabetic retinopathy: An <sup>1</sup>H-NMR-based metabolomic approach using human aqueous humor. *J Pharm Biomed Anal*. 2019; 174:414-421.
  22. Bailey V, Oltmann SC. Trends in radioactive iodine usage at a county hospital: How has practice changed in response to the 2015 American Thyroid Association Guidelines? *J Am Coll Surg*. 2019; 229:e105.
  23. McGreevy A. The changing trend in thyroid surgery in a regional tertiary referral centre: a ten year review of practice. *Br J Surg*. 2011; 98:121-121.
  24. Nikiforov YE, Ohori NP, Hodak SP, Carty SE, Lebeau SO, Ferris RL, Yip L, Seethala RR, Tublin ME, Stang MT. Impact of mutational testing on the diagnosis and management of patients with cytologically indeterminate thyroid nodules: A prospective analysis of 1056 FNA samples. *J Clin Endocrinol Metab*. 2011; 96:3390-3397.
  25. Navascarrillo D, Rodriguez J, Montorogarcia S, Orenespinero E. High-resolution proteomics and metabolomics in thyroid cancer: Deciphering novel biomarkers. *Crit Rev Clin Lab Sci*. 2017; 54:446-457.
  26. Seo JW, Han K, Lee J, Kim E, Moon HJ, Yoon JH, Park VY, Baek H, Kwak JY. Application of metabolomics in prediction of lymph node metastasis in papillary thyroid carcinoma. *PLoS One*. 2018; 13:e0193883.
  27. Torregrossa L, Shintu L, Chandran JN, Tintaru A, Ugolini C, Magalhaes A, Basolo F, Miccoli P, Caldarelli S. Toward the reliable diagnosis of indeterminate thyroid lesions: A HRMAS NMR-based metabolomics case of study. *J Proteome Res*. 2012; 11:3317-3325.
  28. Xu Y, Zheng X, Qiu Y, Jia W, Wang J, Yin S. Distinct metabolomic profiles of papillary thyroid carcinoma and benign thyroid adenoma. *J Proteome Res*. 2015; 14:3315-3321.
  29. Zhou Q, Zhang L, Xie C, Zhang M, Wang Y, Liu G. Metabolomics as a potential method for predicting thyroid malignancy in children and adolescents. *Pediatr Surg Int*. 2020; 36:145-153.
  30. Duarte IF, Gil AM. Metabolic signatures of cancer unveiled by NMR spectroscopy of human biofluids. *Prog Nucl Magn Reson Spectrosc*. 2012; 62:51-74.
  31. Deja S, Dawiskiba T, Balcerzak W, Orczykpawilowicz M, Glod M, Pawelka D, Mlynarz P. Follicular adenomas exhibit a unique metabolic profile. <sup>1</sup>H NMR studies of thyroid lesions. *PLoS One*. 2013; 8:0084637.
  32. Liu X, Zheng X, Du G, Li Z, Qin X. Brain metabonomics study of the antidepressant-like effect of Xiaoyaosan on the CUMS-depression rats by <sup>1</sup>H NMR analysis. *J Ethnopharmacol*. 2019; 235:141-154.
  33. Liu Y, Jia H, Chang X, Ding G, Zhang H, Zou Z M. The metabolic disturbances of isoproterenol induced myocardial infarction in rats based on a tissue targeted metabonomics. *Mol Biosyst*. 2013; 9:2823-2834.
  34. Lecuyer L, Bala AV, Deschasaux M, Bouchemal N, Triba MN, Vasson M, Rossary A, Demidem A, Galan P, Hercberg S. NMR metabolomic signatures reveal predictive plasma metabolites associated with long-term risk of developing breast cancer. *Int J Epidemiol*. 2018; 47:484-494.
  35. Fages A, Duartesalles T, Stepien M, Ferrari P, Fedirko V, Pontoizeau C, Trichopoulou A, Aleksandrova K, Tjonneland A, Olsen A. Metabolomic profiles of hepatocellular carcinoma in a European prospective cohort. *BMC Med*. 2015; 13:242.
  36. Huang J, Mondul AM, Weinstein SJ, Koutros S, Derkach A, Karoly ED, Sampson JN, Moore SC, Berndt SI, Albanes D. Serum metabolomic profiling of prostate cancer risk in the prostate, lung, colorectal, and ovarian cancer screening trial. *Br J Cancer*. 2016; 115:1087-1095.
  37. Mondul AM, Moore SC, Weinstein SJ, Mannisto S, Sampson JN, Albanes D. 1-Stearoylglycerol is associated with risk of prostate cancer: results from a serum metabolomic profiling analysis. *Metabolomics*. 2014; 10:1036-1041.
  38. Stepien M, Duartesalles T, Fedirko V, Floegel A, Barupal DK, Rinaldi S, Achaintre D, Assi N, Tjonneland A, Overvad K. Alteration of amino acid and biogenic amine metabolism in hepatobiliary cancers: Findings from a prospective cohort study. *Int J Cancer*. 2016; 138:348-360.
  39. Li Y, Chen M, Liu C, Xia Y, Xu B, Hu Y, Chen T, Shen M, Tang W. Metabolic changes associated with papillary thyroid carcinoma: A nuclear magnetic resonance-based metabolomics study. *Int J Mol Med*. 2018; 41: 3006-3014.
  40. Miccoli P, Torregrossa L, Shintu L, Magalhaes A, Chandran J, Tintaru A, Ugolini C, Minuto MN, Miccoli M, Basolo F, Caldarelli S. Metabolomics approach to thyroid nodules: A high-resolution magic-angle spinning nuclear magnetic resonance-based study. *Surgery*. 2012; 152:1118-1124.

Received July 31, 2020; Revised August 9, 2020; Accepted August 20, 2020

<sup>§</sup>These authors contributed equally to this work.

\*Address correspondence to:

Shuqi Wang, School of Pharmaceutical Sciences, Shandong University, Jinan, 250012, China.

E-mail: wangsq@sdu.edu.cn

Released online in J-STAGE as advance publication August 27, 2020.